PCCP

PAPER

View Article Online
View Journal | View Issue

Cite this: *Phys. Chem. Chem. Phys.*, 2015, **17**, 31988

Synthesis of hollow cobalt oxide nanopowders by a salt-assisted spray pyrolysis process applying nanoscale Kirkendall diffusion and their electrochemical properties†

Hyeon Seok Ju,[a] Jung Sang Cho,[a] Jong Hwa Kim,[b] Yun Ju Choi[c] and Yun Chan Kang*[a]

Received 14th October 2015,
Accepted 4th November 2015

DOI: 10.1039/c5cp06206c

www.rsc.org/pccp

A new concept for preparing hollow metal oxide nanopowders by salt-assisted spray pyrolysis applying nanoscale Kirkendall diffusion is introduced. The composite powders of metal oxide and indecomposable metal salt are prepared by spray pyrolysis. Post-treatment under a reducing atmosphere and subsequent washing using distilled water produce aggregation-free metal nanopowders. The metal nanopowders are then transformed into metal oxide hollow nanopowders by nanoscale Kirkendall diffusion. Co_3O_4 hollow nanopowders are prepared as first target materials. A cobalt oxide–NaCl composite powder prepared by spray pyrolysis transforms into several Co_3O_4 hollow nanopowders by several treatment processes. The discharge capacities of the Co_3O_4 nanopowders with filled and hollow structures at a current density of 1 A g^{-1} for the 150th cycle are 605 and 775 mA h g^{-1}, respectively. The hollow structure formed by nanoscale Kirkendall diffusion improves the lithium-ion storage properties of Co_3O_4 nanopowders.

Introduction

Nanopowders with hollow structures have received great attention owing to their unique properties and potential application in various fields including energy storage, gas sensors, solar cells, and catalysts.[1–13] Especially, hollow nanopowders with short ion diffusion distances and high structural stability during cycling could be successfully applied to energy storage systems, including lithium- and sodium-ion batteries.[7–18] Hollow nanopowders with single- and multi-components have been mainly prepared by liquid solution processes applying various organic and inorganic templates.[19–24] The removal of the templates by acid etching or calcination results in the hollow nanopowders. However, a more cost-effective process has to be developed for wide application of hollow nanopowders.

Aggregation-free hollow nanopowders have been prepared from metal nanopowders obtained by the liquid solution method applying the Kirkendall effect.[25–31] Cho *et al.* recently reported the synthesis of spherical and nanofiber-type aggregates of hollow nanopowders.[32,33] The nanoscale Kirkendall diffusion process was successfully combined with conventional spray pyrolysis and electrospinning processes. The formation of a carbon matrix embedded with metal nanopowders as intermediate products was the key idea for the spherical and nanofiber-type aggregates of hollow nanopowders.

Spray pyrolysis, which is a gas-phase reaction process, was applied to the preparation of metal oxide nanopowders.[34–38] Okuyama *et al.* reported salt-assisted spray pyrolysis for the preparation of aggregation-free metal oxide nanopowders.[34–37] The composite of a washable metal salt and a metal oxide prepared by spray pyrolysis transformed into metal oxide nanopowders after washing with water. However, the preparation of metal oxide hollow nanopowders has not been carried out using the salt-assisted spray pyrolysis.

In this paper, the preparation of hollow metal oxide nanopowders by salt-assisted spray pyrolysis applying nanoscale Kirkendall diffusion is introduced. Composite powders of metal oxide and indecomposable metal salt were prepared by spray pyrolysis. The composite powder, with particles of several microns in size, transformed into metal oxide hollow nanopowders by applying nanoscale Kirkendall diffusion. The washable metal salt powders embedded with metal nanopowders were prepared by an initial post-treatment process under a reducing atmosphere. The washing of the composite powders using distilled water produced aggregation-free metal nanopowders. The post-treatment of metal

[a] *Department of Materials Science and Engineering, Korea University, Anam-dong, Seongbuk-gu, Seoul 136-713, Korea. E-mail: yckang@korea.ac.kr*
[b] *Daegu Center, Korea Basic Science Institute, 80 Daehakro Bukgu, Daegu 702-701, Republic of Korea*
[c] *Suncheon Center, Korea Basic Science Institute, Suncheon 540-742, Republic of Korea*

† Electronic supplementary information (ESI) available. See DOI: 10.1039/c5cp06206c

nanopowders under an air atmosphere produced the metal oxide hollow nanopowders. This process was first applied to the preparation of Co_3O_4 hollow nanopowders owing to their good electrochemical properties for lithium-ion storage.

Results and discussion

The formation mechanism of the hollow Co_3O_4 nanopowders by salt-assisted spray pyrolysis is shown in Scheme 1. One cobalt oxide–NaCl composite powder was formed from one droplet by drying and decomposition of the metal salt. The post-treatment of the cobalt oxide–NaCl composite powder under a reducing atmosphere produced the Co–NaCl composite powder. The washing of the reduced composite powder using distilled water produced the aggregation-free Co metal nanopowders. Surface oxidation of Co metal nanopowders during the washing process resulted in a Co@Co_3O_4 nanopowder with a core–shell structure. The post-treatment of the Co metal nanopowders under an air atmosphere produced the Co_3O_4 hollow nanopowders by nanoscale Kirkendall diffusion. Small-radius Co cations (Co^{3+} = 75 pm) diffused outward more quickly than the inward diffusion of oxygen anions (O^{2-} = 140 pm). The complete conversion of metallic Co into cobalt oxide by nanoscale Kirkendall diffusion resulted in hollow Co_3O_4 nanopowders.

The formation mechanism of the Co_3O_4 hollow nanopowders by applying salt-assisted spray pyrolysis was investigated based on the morphologies and crystal structures of the powders obtained at each step. The XRD patterns of the powders obtained by salt-assisted spray pyrolysis before and after reduction, shown in Fig. 1a, have sharp peaks for NaCl salt. The powders directly prepared by spray pyrolysis have minor XRD peaks for $NaNO_3$. The small peaks of metallic Co are observed in the XRD pattern of the powders obtained after reduction at 500 °C. The reduction of cobalt oxide resulted in ultrafine Co nanopowders embedded within an indecomposable NaCl matrix. The XRD pattern of the powders obtained after complete washing with distilled water of the Co–NaCl composite powders, shown in Fig. 1b, reveals pure crystalline peaks for metallic Co. The post-treatment of the metallic Co nanopowders under an air atmosphere at temperatures of 300, 400, and 500 °C produced phase-pure Co_3O_4 powders, as shown in Fig. 1b. However, the broad XRD peaks of the powders post-treated at a low temperature of 300 °C reveal the ultrafine crystallite sizes of the Co_3O_4 powders. The mean crystallite sizes of the Co_3O_4 powders post-treated at temperatures of 300, 400, and 500 °C calculated from the width of the (311) peak using the Scherrer equation were 15.2, 17.1, and 19.6 nm, respectively. The mean crystallite size of the filled Co_3O_4 nanopowders prepared as a comparison sample by washing the powders directly prepared by spray pyrolysis at 500 °C was 19.0 nm.

The morphologies of the powders prepared by spray pyrolysis before and after reduction are shown in Fig. 2a and b, respectively. The SEM images reveal the spherical morphology and sizes

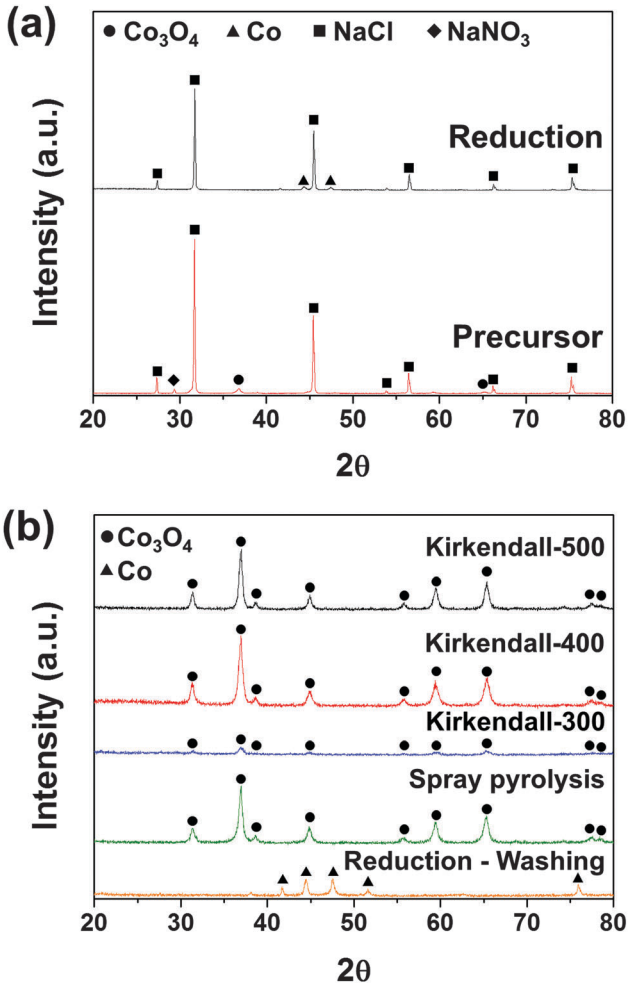

Fig. 1 XRD patterns of (a) the powders obtained by salt-assisted spray pyrolysis before and after the reduction process and (b) the powders obtained after complete washing and post-treatment of the metallic Co nanopowders under an air atmosphere at temperatures of 300, 400, and 500 °C.

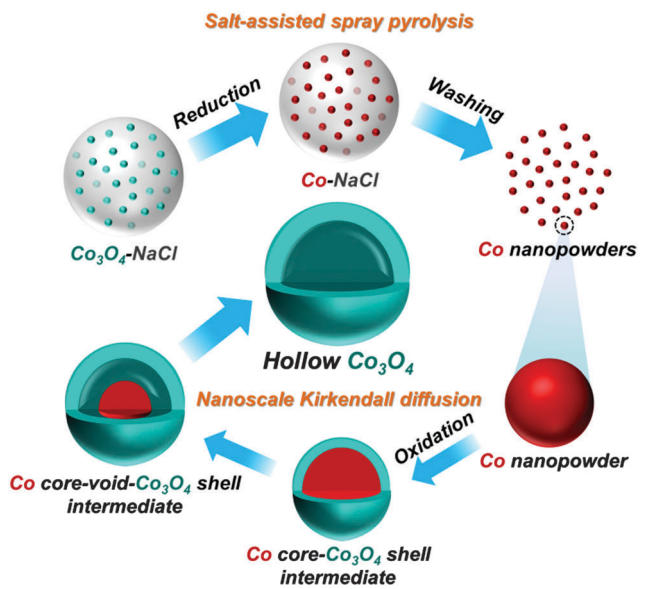

Scheme 1 Schematic diagram for the formation mechanism of the hollow Co_3O_4 nanopowders by salt-assisted spray pyrolysis applying nanoscale Kirkendall diffusion.

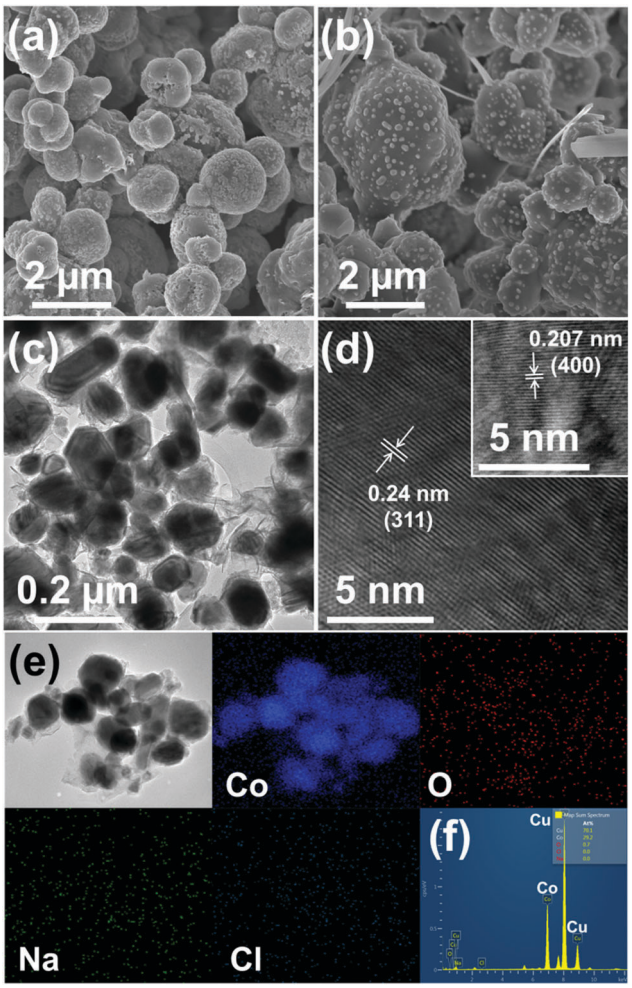

Fig. 2 Morphologies of the powders prepared by spray pyrolysis (a) before and (b) after the reduction process, (c) low and (d) high resolution TEM images, (e) elemental mapping images, and (f) EDAX spectrum of the Co nanopowders obtained after the washing process.

of the two samples; the sizes were on the order of several microns. The TEM images of the metallic Co powders obtained after washing, shown in Fig. 2c and d, reveal a spherical-like morphology and sizes on the order of nanometers. The high-resolution TEM image shown in Fig. 2d shows clear lattice fringes separated by 0.24 and 0.207 nm, which correspond to the (311) and (400) crystal planes of metallic Co. The elemental mapping images shown in Fig. 2e reveal complete reduction of cobalt oxide to metallic Co and complete removal of NaCl by washing. It was difficult to detect oxygen, sodium, and chlorine components in the elemental mapping images.

The morphologies of the nanopowders obtained by post-treatment of the metallic Co nanopowder under an air atmosphere at temperatures of 400 and 500 °C are shown in Fig. 3 and 4, respectively. The nanometer size of the metallic Co nanopowders was well maintained, as observed from the SEM image shown in Fig. 3a. The TEM images shown in Fig. 3b and c reveal the hollow structure of the Co_3O_4 nanopowders. Co nanopowders with dense structures transformed into hollow Co_3O_4 nanopowders by nanoscale Kirkendall diffusion, as described in Scheme 1.

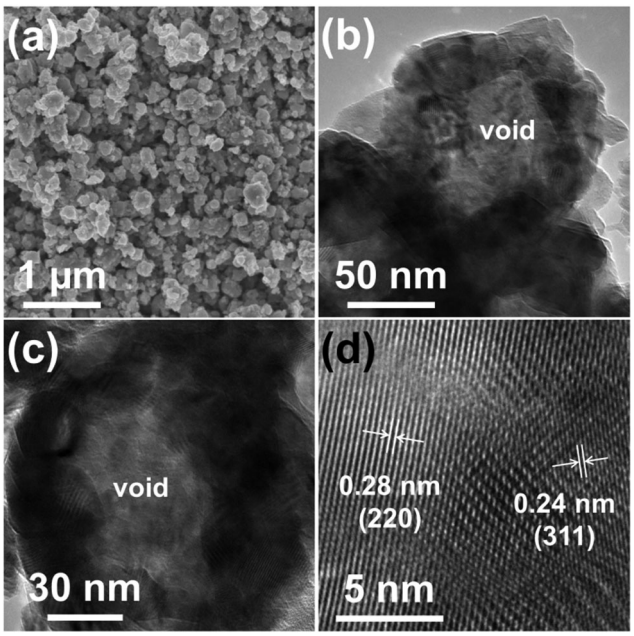

Fig. 3 Morphologies of the nanopowders obtained by post-treatment of the metallic Co nanopowders under an air atmosphere at a temperature of 400 °C: (a) SEM image, (b) and (c) TEM images, and (d) high resolution TEM image.

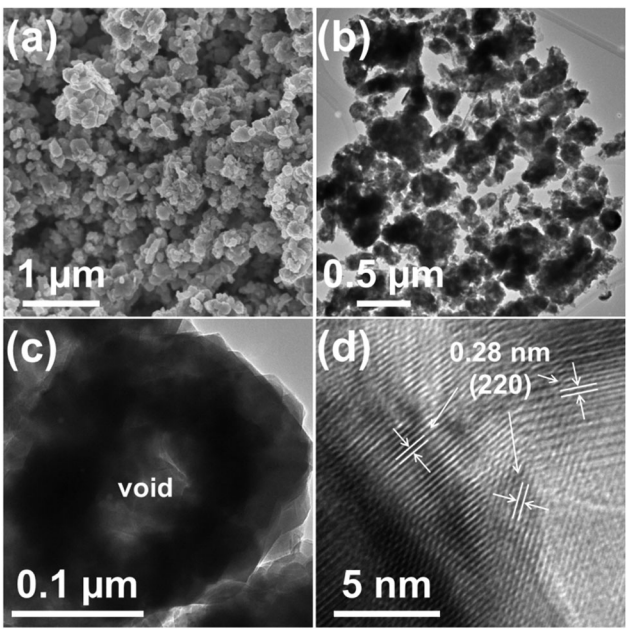

Fig. 4 Morphologies of the nanopowders obtained by post-treatment of the metallic Co nanopowders under an air atmosphere at a temperature of 500 °C: (a) SEM image, (b) and (c) TEM images, and (d) high resolution TEM image.

The high-resolution TEM image shown in Fig. 3d shows clear lattice fringes separated by 0.28 and 0.24 nm, which correspond to the (220) and (311) crystal planes of cubic spinel Co_3O_4 (JCPDS card no. 42-1467). The hollow Co_3O_4 nanopowders were also prepared at a post-treatment temperature of 500 °C by nanoscale Kirkendall diffusion, as shown in Fig. 4. The TEM

image shown in Fig. 4c reveals the well-faceted crystal structure of the hollow Co_3O_4 nanopowder. The high-resolution TEM image shown in Fig. 4d reveals the poly-crystalline crystal structures with ultrafine nanocrystals. The TEM images of the powders obtained at a post-treatment temperature of 300 °C shown in Fig. S2 (ESI†) do not show a clear hollow structure. The dense structure of the metallic Co, shown in Fig. 2, transforms into a porous structure by oxidation to form Co_3O_4. However, incomplete conversion of metallic Co into Co_3O_4 by nanoscale Kirkendall diffusion forms powders with a porous structure. The BET surface areas of the powders obtained by post-treatment of the metallic Co nanopowders under an air atmosphere at temperatures of 300, 400, and 500 °C were 10.8, 9.6, and 10.1 $m^2\ g^{-1}$, respectively. XRD patterns of the powders obtained after post-treatment for 10 and 30 min of the metallic Co nanopowders under an air atmosphere at a temperature of 500 °C are shown in Fig. S3 (ESI†). The complete conversion of metallic cobalt into Co_3O_4 occurred even at a short oxidation time of 10 min. Fig. S4 (ESI†) shows the TEM image of the Co_3O_4 nanopowders obtained after post-treatment for 10 min of the metallic Co nanopowders under an air atmosphere at a temperature of 500 °C. The complete conversion of metallic Co into Co_3O_4 resulted in the hollow structured nanopowder by the nanoscale Kirkendall diffusion process.

The morphologies of the filled Co_3O_4 nanopowders formed by conventional salt-assisted spray pyrolysis are shown in Fig. 5.

Spherical Co_3O_4–NaCl composite powders of several microns in size directly prepared by spray pyrolysis transformed into filled Co_3O_4 nanopowders after washing with distilled water. The TEM image shown in Fig. 5c reveals the well-faceted crystal structure of the filled Co_3O_4 nanopowders. The high-resolution TEM image shown in Fig. 5d shows clear lattice fringes separated by 0.24 and 0.46 nm, which correspond to the (311) and (111) crystal planes of cubic spinel Co_3O_4. The elemental mapping images and EDAX spectrum shown in Fig. 5e and f reveal the complete removal of NaCl by washing. The BET surface area of the filled Co_3O_4 nanopowders is 33.7 $m^2\ g^{-1}$. The N_2 adsorption and desorption isotherms and Barrett–Joyner–Halenda (BJH) pore size distributions of the four samples are shown in Fig. S5 (ESI†). The filled Co_3O_4 nanopowders formed by conventional salt-assisted spray pyrolysis had well-developed mesopores compared with the nanopowders obtained by post-treatment of the metallic Co nanopowders under an air atmosphere at temperatures of 300, 400, and 500 °C. The hollow Co_3O_4 nanopowders prepared by nanoscale Kirkendall diffusion had dense shell structures without pores for gas permeable. However, the mesopores in the filled Co_3O_4 nanopowders formed by conventional salt-assisted spray pyrolysis was due to the hard aggregation between the nanopowders.

The electrochemical properties of the hollow Co_3O_4 nanopowders prepared by nanoscale Kirkendall diffusion are compared with those of the filled Co_3O_4 nanopowders in Fig. 6. The initial discharge and charge curves of the four samples at a current density of 1 A g^{-1} are shown in Fig. 6a. The four samples exhibit similar shapes of initial discharge and charge curves, irrespective of their morphologies. A long plateau region in the initial

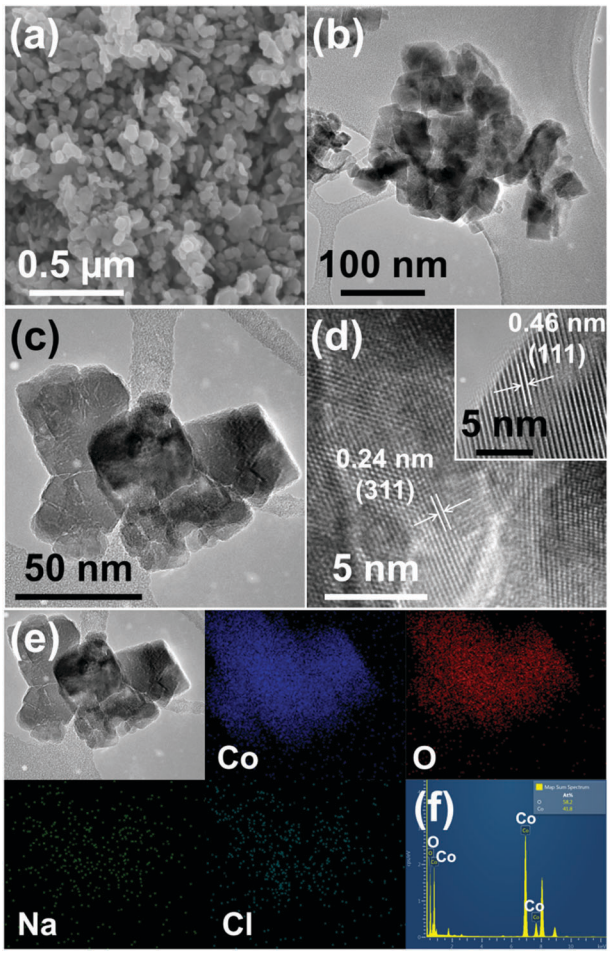

Fig. 5 Morphologies of the filled Co_3O_4 nanopowders formed by conventional salt-assisted spray pyrolysis: (a) SEM image, (b) and (c) TEM images, (d) high resolution TEM image, (e) elemental mapping images, and (f) EDAX spectrum.

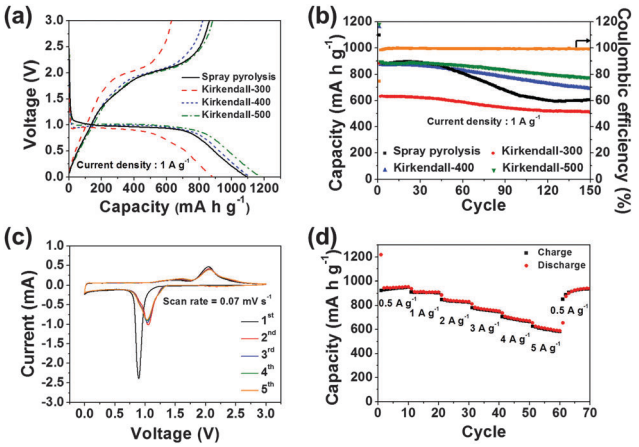

Fig. 6 Electrochemical properties of the powders post-treated at various temperatures: (a) initial charge and discharge curves, (b) cycling performances, (c) CV curves of the powders post-treated at 500 °C, and (d) rate performance of the powders post-treated at 500 °C.

discharge curve at a voltage of approximately 1 V corresponding to Li^+ insertion into the crystal structure of Co_3O_4 and reduction

of the Co ions to Co metal is observed.[39,40] The initial discharge capacities of the powders obtained by post-treatment of the metallic Co nanopowders under an air atmosphere at temperatures of 300, 400, and 500 °C were 884, 1163, and 1182 mA h g^{-1} respectively, and the corresponding charge capacities were 629, 821, and 882 mA h g^{-1}, respectively. The initial discharge and charge capacities of the filled Co_3O_4 nanopowders formed by conventional salt-assisted spray pyrolysis were 1099 and 862 mA h g^{-1}, respectively. The powders obtained by post-treatment of the metallic Co nanopowders under an air atmosphere at a low oxidation temperature of 300 °C had the lowest initial discharge and charge capacities owing to the coexistence of electrochemically inactive metallic Co. The cycling performances of the four samples at a current density of 1 A g^{-1} are shown in Fig. 6b. The discharge capacities of the powders obtained by post-treatment of the metallic Co nanopowders under an air atmosphere at temperatures of 300, 400, and 500 °C for the 150th cycle were 509, 691, and 775 mA h g^{-1}, respectively, and their capacity retentions measured from the second cycle were 80.6, 79.0, and 86.4%, respectively. The discharge capacities of the filled Co_3O_4 nanopowders formed by conventional salt-assisted spray pyrolysis remained constant during the first three cycles, thereafter decreasing continuously to 605 mA h g^{-1} for the 150th cycle. The electrochemical properties of the Co_3O_4 hollow nanopowders showing excellent lithium-ion storage properties were investigated by cyclic voltammograms (CVs). The CVs for the first five cycles at a scan rate of 0.07 mV s^{-1} in the voltage range of 0.001–3 V are shown in Fig. 6c. The sharp reduction peak observed at 0.89 V in the first cathodic sweep is attributed to Li^+ insertion into the crystal structure of Co_3O_4 and the conversion reaction between Co_3O_4 and Li^+ to form metallic Co and Li_2O.[39–42] One oxidation peak observed at approximately 2.0 V is attributed to the oxidation of metallic Co to Co_3O_4 and the decomposition of Li_2O.[41–44] From the second cycle onward, the reduction peak shifted to a higher potential at approximately 1.05 V owing to the conversion of Co_3O_4 into ultrafine nanocrystals during the first cycle.[41,42] The rate performance of the Co_3O_4 hollow nanopowders obtained at an oxidation temperature of 500 °C, in which the current density was increased step-wise from 0.5 to 5 A g^{-1}, is shown in Fig. 6d. The final discharge capacities of the Co_3O_4 hollow nanopowders at current densities of 0.5, 1, 2, 3, 4, and 5 A g^{-1} are 953, 908, 829, 752, 669, and 587 mA h g^{-1}, respectively. The discharge capacities decreased slightly with increasing current densities. The Co_3O_4 hollow nanopowders revealed good rate performance and good capacity recovery when the current density returned to 0.5 A g^{-1}, even after cycling at high current densities.

Electrochemical impedance spectroscopy (EIS) measurements were performed on the hollow and filled Co_3O_4 nanopowders before and after 1 and 100 cycles. The Co_3O_4 hollow nanopowders obtained by an oxidation temperature of 500 °C were used for the EIS measurements. The Nyquist plots shown in Fig. 7 display compressed semicircles in the medium-frequency range, which indicates the charge-transfer resistance (R_{ct}) of the electrode.[45–48] The hollow Co_3O_4 nanopowders with high surface area initially had a slightly higher charge-transfer resistance than the filled

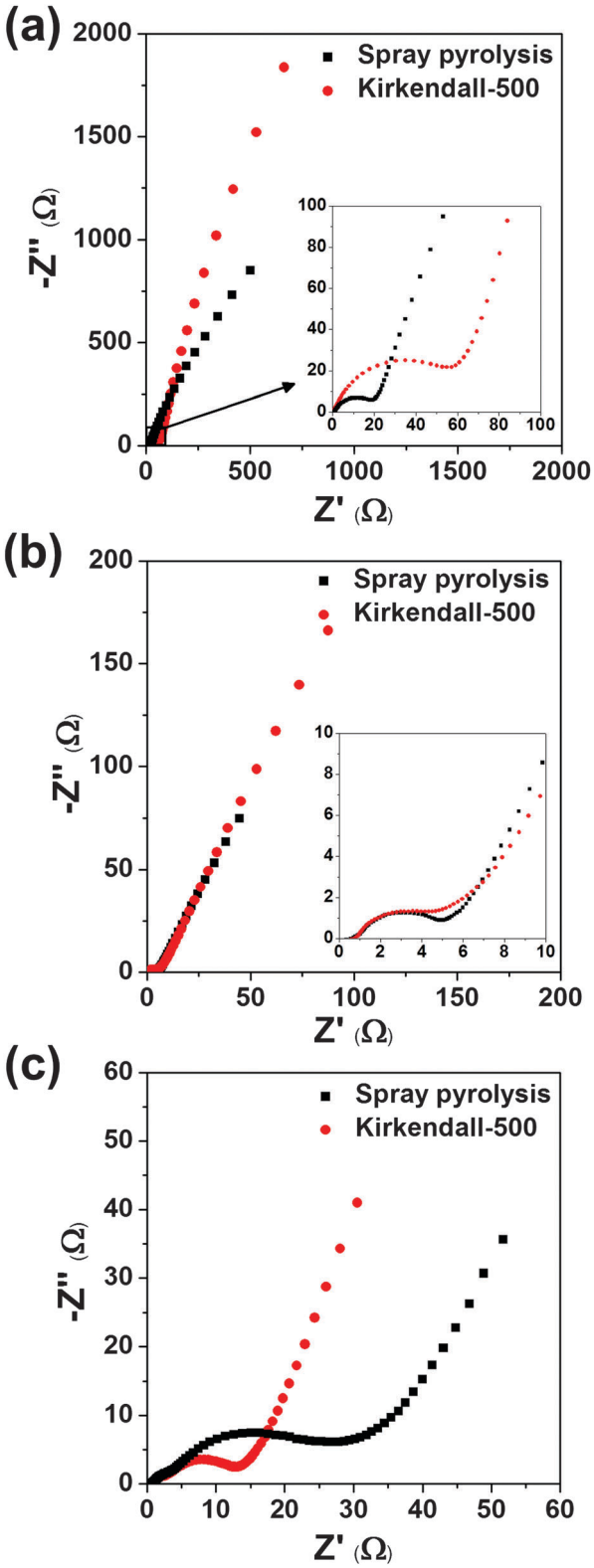

Fig. 7 Nyquist plots of the hollow and filled Co_3O_4 nanopowders: (a) before cycling, (b) after 1 cycle, and (c) after 100 cycles.

Co_3O_4 nanopowders. However, the two samples had similar charge-transfer resistances after the first cycle owing to the conversion of Co_3O_4 into ultrafine nanocrystals during the first

cycle. After 100 cycles, the hollow Co_3O_4 nanopowders had a lower charge-transfer resistance than the filled Co_3O_4 nanopowders. The structural destruction of the filled Co_3O_4 nanopowders during repeated lithium insertion and desertion processes increased their charge-transfer resistance. Therefore, the hollow structure formed by nanoscale Kirkendall diffusion improved the lithium storage properties of the Co_3O_4 nanopowders.

Experimental

Synthesis of hollow Co_3O_4 nanopowders

In this study, cobalt oxide–NaCl composite powders were prepared by the ultrasonic spray pyrolysis process shown in Fig. S1 (ESI†). The spray solutions were obtained by dissolving pre-determined quantities of cobalt nitrate hexahydrate [$Co(NO_3)_2{\cdot}6H_2O$, Junsei] and NaCl in distilled water. Indecomposable NaCl with a high melting temperature of 801 °C was applied as a water-washable metal salt. The concentrations of cobalt nitrate hexahydrate and NaCl were fixed at 0.09 and 0.9 M, respectively. The pyrolysis was carried out in a quartz reactor 1200 mm in length and 50 mm in diameter and the reactor temperature was maintained at 500 °C. Nitrogen was used as the carrier gas at a flow rate of 40 L min^{-1}. The precursor powders obtained by spray pyrolysis were post-treated at 500 °C in a 10% H_2/Ar gas mixture for 3 h and subsequently washed with distilled water three times to remove the washable NaCl. The Co nanopowders were transformed into Co_3O_4 hollow nanopowders by post-treatment at temperatures of 300, 400, and 500 °C in air for 3 h. Filled Co_3O_4 nanopowders were also prepared as comparison samples by washing the powders directly prepared by spray pyrolysis at 500 °C. For simplicity, the Co_3O_4 nanopowders formed by post-treatment at temperatures of 300, 400, and 500 °C are referred to as ''Kirkendall-300'', ''Kirkendall-400'', and ''Kirkendall-500'' nanopowders, respectively.

Characterization

The crystal structures of the powders were investigated using X-ray diffractometry (XRD, X'pert PRO MPD) with Cu Kα radiation (λ = 1.5418 Å) at the Korea Basic Science Institute (Daegu). The morphologies of the powders were investigated using field-emission scanning electron microscopy (FE-SEM, Hitachi S-4800) and high-resolution transmission electron microscopy (HR-TEM, JEOL JEM-2100F) at a working voltage of 200 kV. The specific surface areas of the powders were calculated by a Brunauer–Emmett–Teller (BET) analysis of nitrogen adsorption measurements (TriStar 3000).

Electrochemical measurements

The electrochemical properties of the Co_3O_4 hollow nanopowders were analyzed by constructing a 2032-type coin cell. The anode was prepared by mixing the active material, carbon black, and sodium carboxymethyl cellulose (CMC) in a weight ratio of 7 : 2 : 1. Li metal and microporous polypropylene film were used as the counter electrode and the separator, respectively. The electrolyte was 1 M $LiPF_6$ dissolved in a mixture of fluoroethylene carbonate/dimethyl carbonate (FEC/DMC; 1 : 1 v/v). The discharge/charge characteristics of the samples were investigated by cycling in a 0.001–3 V potential range at various current densities. Cyclic voltammograms were measured at a scan rate of 0.07 mV s^{-1}.

Conclusions

Cobalt oxide hollow nanopowders were prepared by salt-assisted spray pyrolysis applying nanoscale Kirkendall diffusion. Filled cobalt nanopowders formed by salt-assisted spray pyrolysis transformed into hollow cobalt oxide nanopowders by nanoscale Kirkendall diffusion. The electrochemical properties of the hollow Co_3O_4 nanopowders were compared with those of the filled Co_3O_4 nanopowders prepared by salt-assisted spray pyrolysis. The hollow structure formed by nanoscale Kirkendall diffusion improved the lithium storage properties of the Co_3O_4 nanopowders by enhancing the structural stability during cycling. Salt-assisted spray pyrolysis could thus be applied to the preparation of metal oxide hollow nanopowders with various compositions for wide applications, including energy storage.

Acknowledgements

This work was supported by the Energy Efficiency & Resources Core Technology Program of the Korea Institute of Energy Technology Evaluation and Planning (KETEP), granted financial resource from the Ministry of Trade, Industry & Energy, Republic of Korea (201320200000420).

References

1 Y. G. Guo, J. S. Hu and L. J. Wan, *Adv. Mater.*, 2008, **20**, 2878–2887.
2 Y. Yao, M. T. McDowell, I. Ryu, H. Wu, N. Liu, L. Hu, W. D. Nix and Y. Cui, *Nano Lett.*, 2011, **11**, 2949–2954.
3 X. Lai, J. Li, B. A. Korgel, Z. Dong, Z. Li, F. Su, J. Du and D. Wang, *Angew. Chem., Int. Ed.*, 2011, **123**, 2790–2793.
4 S. Liu, Z. Wang, C. Yu, H. B. Wu, G. Wang, Q. Dong, J. Qiu and A. Eychmüller, *Adv. Mater.*, 2013, **25**, 3462–3467.
5 H. Wu, M. Xu, H. Wu, J. Xu, Y. Wang, Z. Peng and G. J. Zheng, *Mater. Chem.*, 2012, **22**, 19821–19825.
6 H. Wang, L. F. Cui, Y. Yang, H. Sanchez Casalongue, J. T. Robinson, Y. Liang, Y. Cui and H. Dai, *J. Am. Chem. Soc.*, 2010, **132**, 13978–13980.
7 L. Zhou, H. Xu, H. Zhang, J. Yang, S. B. Hartono, K. Qian, J. Zou and C. Yu, *Chem. Commun.*, 2013, **49**, 8695–8697.
8 X. Zhou, Y. X. Yin, L. J. Wan and Y. G. Guo, *J. Mater. Chem.*, 2012, **22**, 17456–17459.
9 C. Niu, J. Meng, C. Han, K. Zhao, M. Yan and L. Mai, *Nano Lett.*, 2014, **14**, 2873–2878.
10 H. Wu, M. Xu, Y. Wang and G. Zheng, *Nano Res.*, 2013, **6**, 167–173.

11 Y. Zhong, L. Su, M. Yang, J. Wei and Z. Zhou, *ACS Appl. Mater. Interfaces*, 2013, **5**, 11212–11217.
12 X. W. Lou, L. A. Archer and Z. Yang, *Adv. Mater.*, 2008, **20**, 3987–4019.
13 X. H. Xia, J. P. Tu, X. L. Wang, C. D. Gu and X. B. Zhao, *Chem. Commun.*, 2011, **47**, 5786–5788.
14 X. Wang, X. L. Wu, Y. G. Guo, Y. Zhong, X. Cao, Y. Ma and J. Yao, *Adv. Funct. Mater.*, 2010, **20**, 1680–1686.
15 J. Zhu, Z. Yin, D. Yang, T. Sun, H. Yu, H. E. Hoster, H. H. Hng, H. Zhang and Q. Yan, *Energy Environ. Sci.*, 2013, **6**, 987–993.
16 M. Xu, L. Kong, W. Zhou and H. Li, *J. Phys. Chem. C*, 2007, **111**, 19141–19147.
17 X. M. Yin, C. C. Li, M. Zhang, Q. Y. Hao, S. Liu, L. B. Chen and T. H. Wang, *J. Phys. Chem. C*, 2010, **114**, 8084–8088.
18 B. Koo, H. Xiong, M. D. Slater, V. B. Prakapenka, M. Balasubramanian, P. Podsiadlo, C. S. Johnson, T. Rajh and E. V. Shevchenko, *Nano Lett.*, 2012, **12**, 2429–2435.
19 L. Zhang, H. B. Wu and X. W. Lou, *J. Am. Chem. Soc.*, 2013, **135**, 10664–10672.
20 R. Wu, X. Qian, K. Zhou, J. Wei, J. Lou and P. M. Ajayan, *ACS Nano*, 2014, **8**, 6297–6303.
21 W. S. Kim, Y. Hwa, H. C. Kim, J. H. Choi, H. J. Sohn and S. H. Hong, *Nano Res.*, 2014, **7**, 1128–1136.
22 M. Sasidharan, N. Gunawardhana, C. Senthil and M. Yoshio, *J. Mater. Chem. A*, 2014, **2**, 7337–7344.
23 J. Hu, M. Chen, X. Fang and L. Wu, *Chem. Soc. Rev.*, 2011, **40**, 5472–5491.
24 X. M. Sun, J. F. Liu and Y. D. Li, *Chem. – Eur. J.*, 2006, **12**, 2039–2047.
25 W. Wang, M. Dahl and Y. Yin, *Chem. Mater.*, 2013, **25**, 1179–1189.
26 Y. Yu, X. Yin, A. Kvit and X. Wang, *Nano Lett.*, 2014, **14**, 2528–2535.
27 B. D. Anderson and J. B. Tracy, *Nanoscale*, 2014, **6**, 12195–12216.
28 Y. M. Lee, M. R. Jo, K. S. Song, K. M. Nam, J. T. Park and Y. M. Kang, *ACS Appl. Mater. Interfaces*, 2012, **4**, 3459–3464.
29 Y. Yin, R. M. Rioux, C. K. Erdonmez, S. Hughes, G. A. Somorjai and A. P. Alivisatos, *Science*, 2004, **304**, 711–714.
30 R. K. Chiang and R. T. Chiang, *Inorg. Chem.*, 2007, **46**, 369–371.
31 H. J. Fan, M. Knez, R. Scholz, D. Hesse, K. Nielsch, M. Zacharias and U. Gösele, *Nano Lett.*, 2007, **7**, 993–997.
32 J. S. Cho, Y. J. Hong and Y. C. Kang, *ACS Nano*, 2015, **9**, 4026–4035.
33 J. S. Cho, Y. J. Hong, J. H. Lee and Y. C. Kang, *Nanoscale*, 2015, **7**, 8361–8367.
34 B. Xia, I. W. Lenggoro and K. Okuyama, *Adv. Mater.*, 2001, **13**, 1579–1582.
35 Y. Itoh, I. W. Lenggoro, S. E. Pratsinis and K. Okuyama, *J. Mater. Res.*, 2002, **17**, 3222–3229.
36 K. Okuyama and I. W. Lenggoro, *Chem. Eng. Sci.*, 2003, **58**, 537–547.
37 B. Xia, I. W. Lenggoro and K. Okuyama, *J. Mater. Chem.*, 2001, **11**, 2925–2927.
38 X. Zhang, W. Jiang, D. Song, H. Sun, Z. Sun and F. Li, *J. Alloys Compd.*, 2009, **475**, L34–L37.
39 P. Poizot, S. Laruelle, S. Grugeon, L. Dupont and J. M. Tarascon, *Nature*, 2000, **407**, 496–499.
40 J. G. Kang, Y. D. Ko, J. G. Park and D. W. Kim, *Nanoscale Res. Lett.*, 2008, **3**, 390–394.
41 X. Yao, X. Xin, Y. Zhang, J. Wang, Z. Liu and X. Xu, *J. Alloys Compd.*, 2012, **521**, 95–100.
42 L. Zhan, Y. Wang, W. Qiao, L. Ling and S. Yang, *Electrochim. Acta*, 2012, **78**, 440–445.
43 M. M. Rahmana, J. Z. Wang, X. L. Deng, Y. Li and H. K. Liu, *Electrochim. Acta*, 2009, **55**, 504–510.
44 F. Wang, C. Lu, Y. Qin, C. Liang, M. Zhao, S. Yang, Z. Sun and X. Song, *J. Power Sources*, 2013, **235**, 67–73.
45 M. S. Park, Y. M. Kang, G. X. Wang, S. X. Dou and H. K. Liu, *Adv. Funct. Mater.*, 2008, **18**, 455–461.
46 S. H. Choi and Y. C. Kang, *ChemSusChem*, 2013, **6**, 2111–2116.
47 Y. Zhu, Y. Xu, Y. Liu, C. Luo and C. Wang, *Nanoscale*, 2013, **5**, 780–787.
48 Y. N. Ko, S. B. Park, K. Y. Jung and Y. C. Kang, *Nano Lett.*, 2013, **13**, 5462–5466.

